The Distance to NGC 4993

The Host Galaxy of the Gravitational-wave Event GW170817

Hjorth, Jens; Levan, Andrew J.; Tanvir, Nial R.; Lyman, Joe D.; Wojtak, Radoslaw; Schroder, Sophie L.; Mandel, Ilya; Gall, Christa; Bruun, Sofie H.

Published in:
Astrophysics Journal Letters

DOI:
10.3847/2041-8213/aa9110

Publication date:
2017

Document version
Publisher's PDF, also known as Version of record

The Astrophysical Journal Letters, 848:L31 (6pp), 2017 October 20 https://doi.org/10.3847/2041-8213/aa9110

The Distance to NGC 4993: The Host Galaxy of the Gravitational-wave Event GW170817

Jens Hjorth[1], Andrew J. Levan[2], Nial R. Tanvir[3], Joe D. Lyman[2], Radosław Wojtak[1], Sophie L. Schrøder[1], Ilya Mandel[4], Christa Gall[1], and Sofie H. Bruun[1]
[1] Dark Cosmology Centre, Niels Bohr Institute, University of Copenhagen, Juliane Maries Vej 30, DK-2100 Copenhagen Ø, Denmark
[2] Department of Physics, University of Warwick, Coventry CV4 7AL, UK
[3] Department of Physics and Astronomy, University of Leicester, Leicester LE1 7RH, UK
[4] Birmingham Institute for Gravitational Wave Astronomy and School of Physics and Astronomy, University of Birmingham, Birmingham B15 2TT, UK
Received 2017 September 29; revised 2017 October 2; accepted 2017 October 3; published 2017 October 16

Abstract

The historic detection of gravitational waves from a binary neutron star merger (GW170817) and its electromagnetic counterpart led to the first accurate (sub-arcsecond) localization of a gravitational-wave event. The transient was found to be $\sim 10''$ from the nucleus of the S0 galaxy NGC 4993. We report here the luminosity distance to this galaxy using two independent methods. (1) Based on our MUSE/VLT measurement of the heliocentric redshift ($z_{\rm helio} = 0.009783 \pm 0.000023$), we infer the systemic recession velocity of the NGC 4993 group of galaxies in the cosmic microwave background (CMB) frame to be $v_{\rm CMB} = 3231 \pm 53$ km s^{-1}. Using constrained cosmological simulations we estimate the line-of-sight peculiar velocity to be $v_{\rm pec} = 307 \pm 230$ km s^{-1}, resulting in a cosmic velocity of $v_{\rm cosmic} = 2924 \pm 236$ km s^{-1} ($z_{\rm cosmic} = 0.00980 \pm 0.00079$) and a distance of $D_z = 40.4 \pm 3.4$ Mpc assuming a local Hubble constant of $H_0 = 73.24 \pm 1.74$ km s^{-1} Mpc^{-1}. (2) Using *Hubble Space Telescope* measurements of the effective radius ($15\farcs5 \pm 1\farcs5$) and contained intensity and MUSE/VLT measurements of the velocity dispersion, we place NGC 4993 on the Fundamental Plane (FP) of E and S0 galaxies. Comparing to a frame of 10 clusters containing 226 galaxies, this yields a distance estimate of $D_{\rm FP} = 44.0 \pm 7.5$ Mpc. The combined redshift and FP distance is $D_{\rm NGC\ 4993} = 41.0 \pm 3.1$ Mpc. This "electromagnetic" distance estimate is consistent with the independent measurement of the distance to GW170817 as obtained from the gravitational-wave signal ($D_{\rm GW} = 43.8^{+2.9}_{-6.9}$ Mpc) and confirms that GW170817 occurred in NGC 4993.

Key words: galaxies: distances and redshifts – galaxies: fundamental parameters – galaxies: individual (NGC 4993)

1. Introduction

GW170817 was the first gravitational-wave event arising from a binary neutron star (NS) merger to have been detected by LIGO/Virgo (Abbott et al. 2017a). The source was localized to a sky region of 28 deg^2 purely using gravitational-wave data from the three interferometers. As such, it provided the first realistic chance of detecting an electromagnetic counterpart, as outlined in Abbott et al. (2017b): 2 s after the merger, *Fermi* and *INTEGRAL* detected a weak gamma-ray burst, and half a day after the event, an optical (Coulter et al. 2017) and near-infrared (NIR; Tanvir et al. 2017) counterpart was localized to sub-arcsecond precision, $\sim 10''$ from the nucleus of the S0 galaxy NGC 4993 (Abbott et al. 2017b). It exhibited an unprecedented optical/NIR lightcurve and spectral evolution (Abbott et al. 2017b; Tanvir et al. 2017), strongly suggestive of formation of very heavy elements (lanthanides) out of the tidally ejected neutron-rich material in the merger (Pian et al. 2017; Tanvir et al. 2017).

It is highly likely that the neutron star–neutron star (NS–NS) merger occurred in NGC 4993. A precise distance to NGC 4993 is therefore required in order to understand the energetics of the event. Furthermore, since NS–NS mergers provide a route to H_0 via the direct "standard siren" measurement provided by the Abbott et al. (2017c), it is valuable to have an accurate redshift as well as independent electromagnetic distance estimates. The redshift, especially if corrected to the Hubble flow, is vital in constructing the gravitational-wave Hubble diagram, while an independent distance estimate can confirm the galaxy association.

To our knowledge, there are no direct measurements of the distance to NGC 4993 (Tully et al. 2009). NGC 4993 belongs to a group of galaxies (see Section 3.2). Two galaxies have distances in the Cosmicflows-3 data release (Tully et al. 2016). NGC 4970 (PGC 45466) has a Fundamental Plane (FP) distance of 39.8 ± 10.3 Mpc from the 6dF Galaxy Survey (Springob et al. 2014), while ESO508-G019 (PGC 45666) has a Tully–Fisher distance of 37.5 ± 5.6 Mpc from *I*-band and *Spitzer* photometry (Willick et al. 1997; Springob et al. 2009; Sorce et al. 2014). Combined, these estimates suggest a group distance of 38.0 ± 4.9 Mpc.

Section 2 summarizes the origin of the data used to provide new distance estimates to NGC 4993. In Section 3, we provide an updated distance along this avenue. We use a new redshift and estimate of the peculiar velocity of NGC 4993. In Section 4, we obtain the first direct estimate of the distance to NGC 4993 itself using the FP method. We discuss the results in Section 5 and summarize in Section 6.

2. Data

The data used in this Letter are described in Levan et al. (2017). NGC 4993 was observed with the Very Large Telescope (VLT) and the MUSE Integral Field Spectrograph on 2017 August 18.

We also used an Advanced Camera for Surveys F606W *Hubble Space Telescope* (*HST*) image of NGC 4993 obtained on 2017 April 28. The image was reduced via `astrodrizzle`, with the final scale set to $0\farcs07$.

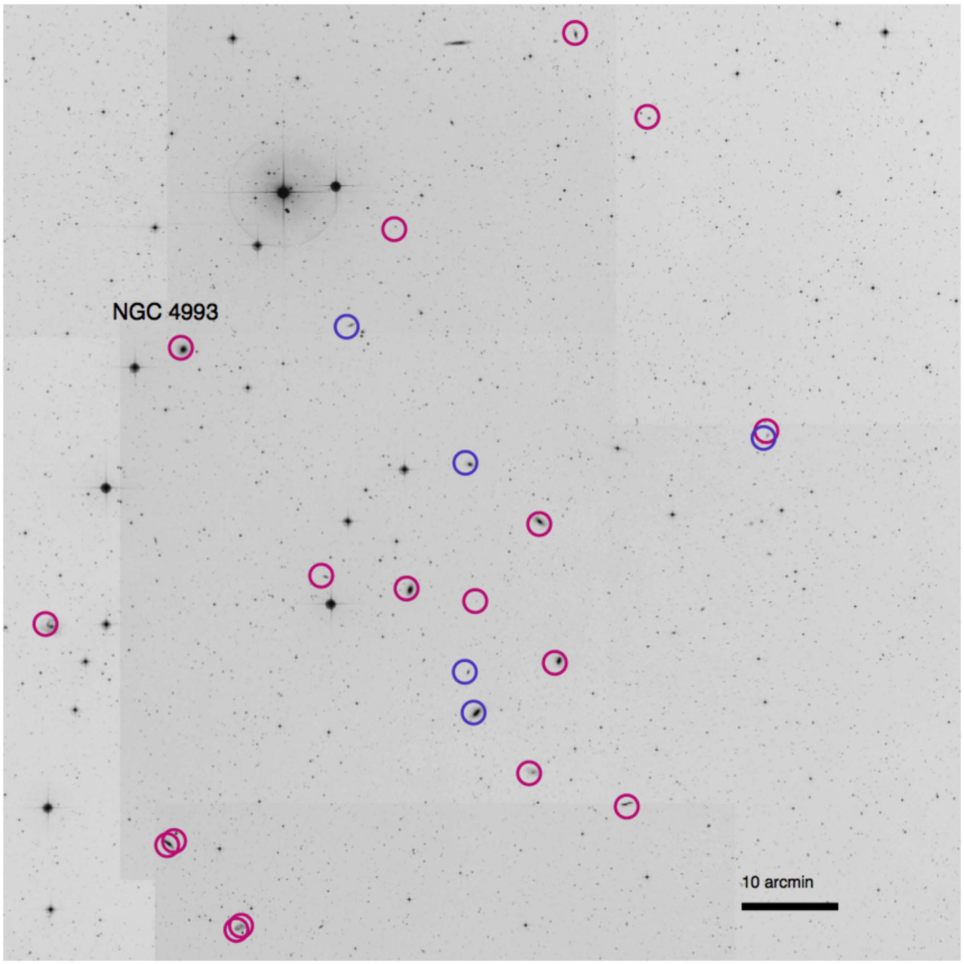

Figure 1. Members of the NGC 4993 group of galaxies. Purple circles indicate Kourkchi & Tully (2017) group galaxies with heliocentric velocities less than 3005 km s^{-1}, while blue circles indicate galaxies with heliocentric velocities larger than 3169 km s^{-1} (see Figure 2). This Digitized Sky Survey image is 2 deg on the side. North is up, and east is to the left.

3. Redshift Distance

3.1. Redshift of NGC 4993

An updated value of the heliocentric redshift of NGC 4993 is obtained from the MUSE/VLT observation reported by Levan et al. (2017). Based on fits to the absorption lines from stars in the center of the galaxy, the heliocentric recession velocity is determined to be $v_{\rm helio} = 2933 \pm 7$ km s^{-1}, corresponding to a heliocentric redshift of $z_{\rm helio} = 0.009783 \pm 0.000023$.

3.2. Redshift of the NGC 4993 Group of Galaxies

NGC 4993 appears to be a member of a group of galaxies; see Figure 1. Crook et al. (2007) list it to be one of 46 members of a group of galaxies in the 2MASS redshift survey (group number 955, with an average heliocentric velocity of 2558 km s^{-1} and a velocity dispersion of 486.5 km s^{-1}). However, NGC 4993 is located ≈4.2 Mpc in projection from the center of this putative group and a non-detection in X-rays appears to rule out such a rich relaxed group. Makarov & Karachentsev (2011) find NGC 4993 to be one of 15 members with a velocity dispersion of 74 km s^{-1}. Recently, Kourkchi & Tully (2017) found it to be one of 22 members of a group with a mean heliocentric velocity of 2995 km s^{-1} and a velocity dispersion of 118 km s^{-1} (our calculation of the rms velocity spread of the 22 galaxies is 155 km s^{-1}). However, it is evident from Figure 2 that five of the galaxies have a much higher recession velocity than the rest and so do not appear to be part of a relaxed group. We therefore exclude these 5 galaxies and consider the properties of the remaining 17 galaxies. We also update the NGC 4993 velocity from 2902 to 2933 km s^{-1} (as measured here) and compute a mean heliocentric velocity of 2921 km s^{-1} and a velocity dispersion of 53 km s^{-1}. This small velocity dispersion and the large extent of the structure suggest a relaxation time larger than 10^{10} years, and so the structure is unlikely to be a relaxed group. We therefore adopt the velocity dispersion of the structure as the uncertainty in the recession velocity (rather than the error in the mean, $53/\sqrt{16} = 13$ km s^{-1}), i.e., $v_{\rm NGC\ 4993,group} = 2921 \pm 53$ km s^{-1}. This structure is shown in Figure 1. Note that NGC 4993 is at the outskirts of the structure while its velocity is very close to the mean velocity of the structure.

Using the *WMAP* measurement of the cosmic microwave background (CMB) dipole (Hinshaw et al. 2009), we obtain[5] a recession velocity in the frame defined by the CMB of $v_{\rm CMB} = 3231 \pm 53$ km s^{-1}.

[5] Using the NED Velocity Correction Calculator at https://ned.ipac.caltech.edu/forms/vel_correction.html.

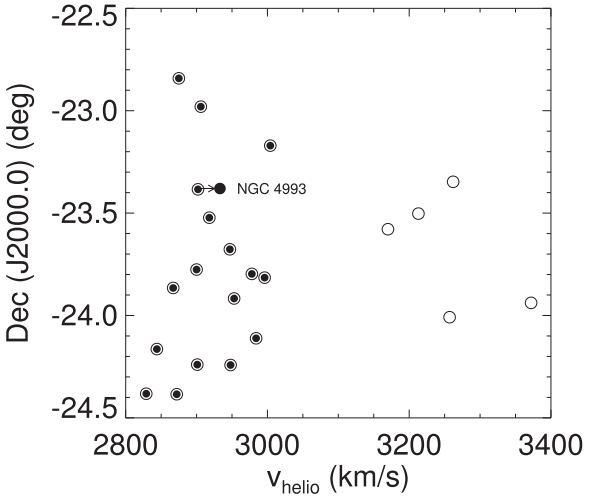

Figure 2. Heliocentric velocities of the Kourkchi & Tully (2017) group PCG1 45466 containing NGC 4993. There is a clear gap in the heliocentric velocities, with no galaxies in the range 3005–3169 km s^{-1}, i.e., in the positive range above the mean velocity $v_{\rm helio} = 2995$ km s^{-1}. Considering only galaxies plotted as filled circles, the mean velocity is $v_{\rm helio} = 2921$ km s^{-1}. The updated velocity of NGC 4993 is indicated.

3.3. Peculiar Velocity

To estimate the "cosmic velocity," i.e., the recession velocity corresponding to pure Hubble flow, we need to take into account the peculiar velocity due to large-scale structure:

$$v_{\rm cosmic} = v_{\rm CMB} - v_{\rm pec}. \quad (1)$$

Following Li et al. (2014), we make use of a dark-matter simulation from the Constrained Local Universe Simulations (CLUES) project to find the best estimate of the peculiar velocity of NGC 4993. The initial conditions of the simulation were generated using constraints from observations probing the distribution of galaxies and their peculiar velocities so that the final snapshot is a 3D representation of the observed local universe (for technical details see Gottloeber et al. 2010). The simulation reproduces all main large-scale structures around the Local Group such as the Virgo cluster, the Coma cluster, the Great Attractor, and the Perseus–Pisces supercluster and the resulting peculiar velocity field. Structures on scales smaller than $\sim 5h^{-1}$ Mpc are not subject to observational constraints and emerge from random sampling of the initial density field. Their evolution, however, is strongly influenced by tidal forces from the nearby large-scale structures. Therefore, the simulation provides a realistic and dynamically self-consistent model for the matter distribution and the velocity field in the local universe. The simulation adopted cosmological parameters from the third data release of the *WMAP* satellite (WMAP3), i.e., matter density $\Omega_m = 0.24$, dimensionless Hubble parameter $h = 0.73$, and normalization of the power spectrum $\sigma_8 = 0.76$. The simulation box has a side length equal to 160 h^{-1} Mpc and contains 1024^3 particles.

In order to find the position vector of the observational cone in the simulation box, we calculate the angular distances of NGC 4993 from three reference points that have unambiguous analogs in the numerical model: the direction of the peculiar velocity of the Local Group, the Great Attractor (Norma cluster), and the Perseus cluster. These three angular separations are then used to determine the position vector with respect to the analog of the Local Group in the simulation box. Having found the direction of NGC 4993 in the simulation, we compute the radial projection of peculiar velocities of dark-matter particles found in a narrow light cone. Figure 3 shows the resulting projected peculiar velocity as a function of the recession velocity measured in the reference frame of the CMB with respect to an observer located in the Local Group. For the sake of readability, we downsampled from the selected dark-matter particles. The peculiar velocities result primarily from the proximity of the Great Attractor (49° from NGC 4993).

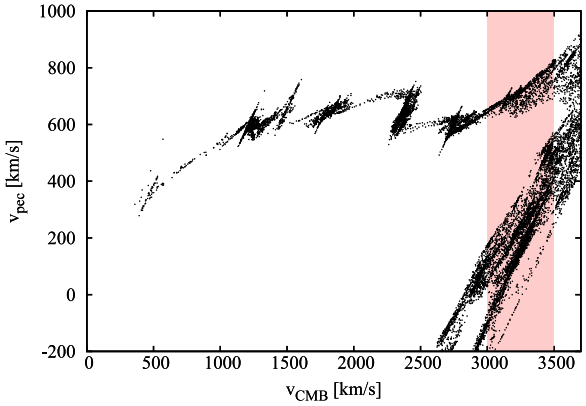

Figure 3. Peculiar velocities (line-of-sight component) of dark-matter particles in the constrained simulation, in the direction of NGC 4993. Velocity $v_{\rm CMB}$ is measured in the reference frame of the CMB with respect to an observer located at the Local Group (numerical analog). The red stripe indicates the location of NGC 4993.

Using a ± 250 km s^{-1} velocity range centered at the measured CMB rest-frame velocity of NGC 4993, i.e., $v_{\rm CMB} = 3231$ km s^{-1}, we find a mean peculiar velocity $v_{\rm pec} = 307$ km s^{-1} and an rms $\sigma_{\rm pec} = 230$ km s^{-1}. The adopted range corresponds to the smallest scale constrained by the observational data ($\sim 5\ h^{-1}$ Mpc).

Combining $\sigma_{\rm pec}$ with the error in group velocity the final cosmic velocity is $v_{\rm cosmic} = 2924 \pm 236$ km s^{-1}.

3.4. Hubble Distance

To a good approximation, Hubble's law gives the luminosity distance at low redshift as

$$D_z = H_0^{-1} c z_{\rm cosmic}\left(1 + \frac{1 - q_0}{2} z_{\rm cosmic}\right), \quad (2)$$

with $q_0 = -0.53$ for standard cosmological parameters. For a local Hubble constant of $H_0 = 73.24 \pm 1.74$ km s^{-1} Mpc^{-1} (Riess et al. 2016) we obtain $D_z = 40.4 \pm 3.4$ Mpc. The quoted uncertainty accounts for the limited depth of the NGC 4993 group of galaxies (Figure 1), which is less than 1°, corresponding to 0.6 Mpc.

We note that adopting a mean heliocentric velocity of 2995 km s^{-1} for the NGC 4993 group (Kourkchi & Tully 2017) would increase $v_{\rm cosmic}$ by 74 km s^{-1} and hence the inferred distance by 1.0 Mpc.

4. FP Distance

The FP is a fairly tight relation between radius, surface brightness, and velocity dispersion for bulge-dominated galaxies (Djorgovski & Davis 1987). It is widely used as a

distance indicator for early-type galaxies. The FP that we consider is

$$\log R_e + \alpha \log \sigma + \beta \log \langle I_r \rangle_e + \gamma, \quad (3)$$

where R_e is the effective radius measured in arcseconds, σ is the velocity dispersion in km s^{-1}, $\langle I_r \rangle_e$ is the mean intensity inside the effective radius measured in $L_\odot$ pc^{-2}, and γ is the distance-dependent zero point of the relation.

The global values adopted by Jorgensen et al. (1996) are $\alpha = 1.24$ and $\beta = 0.82$ in Gunn r. We adopt $r = \mathrm{F606W} + 0.04$ mag (Fukugita et al. 1995; Sirianni et al. 2005) for E/S0 galaxies. The surface brightness is

$$\log \langle I_r \rangle_e = -0.4[\mathrm{F606W}(<R_e) + 0.04 - 0.29 + 2.5 \log \pi + 5 \log R_e - 26.40 - 10 \log(1+z) - 2.5 \log(1+z)],$$

(Hjorth & Tanvir 1997), which transforms into Gunn r and corrects for Galactic extinction (Schlafly & Finkbeiner 2011), cosmological surface brightness dimming, and spectral bandwidth (k-correction), with $z = z_{\mathrm{cosmic}}$.

In principle, FP distances may be affected by the observed magnitude range, morphological makeup of the sample (E-to-S0 ratio), and environment. According to Jorgensen et al. (1996), their version of the FP excludes biases above 1% due to magnitude and morphological selection.

4.1. FP Parameters

4.1.1. Photometric Properties

The *HST* F606W image is fit to a 2D version of the Sérsic function,

$$I(R) = I_e \exp\left\{-b_n\left[\left(\frac{R}{R_e}\right)^{\frac{1}{n}} - 1\right]\right\}, \quad (4)$$

where R_e is the half-light (effective) radius, I_e is the intensity at R_e, and n is the fitted Sérsic index (which is uniquely related to the coefficient b_n).

The fit was performed using the Astropy package `FittingWithOutlierRemoval` (Astropy Collaboration 2013). The function uses σ clipping to filter out bad data points and iterates n_{iter} times over the data. Data deviating more than n_σ times the standard deviation of surrounding data points are removed in each iteration. The filtered data are then fitted with the Sérsic function.

The fitting algorithm was applied to a range of different combinations of n_{iter} and n_σ. Fitting parameters stabilize after 15 iterations for all n_σ values, so $n_{\mathrm{iter}} = 15$ is used for the fit. The final n_σ was chosen for values excluding outliers and including most of the light from the center of the galaxy. This worked well for n_σ values between 20 and 40.

An example of a fit to the F606W image is shown in Figure 4. Inside an effective radius of $15\farcs5$ we find F606W = 12.99 mag. The Sérsic index is $n \approx 3.8$. A detailed discussion of the properties of NGC 4993 is presented in Levan et al. (2017).

4.1.2. Velocity Dispersion

The velocity dispersion is measured in an aperture equivalent to $3\farcs4$ at Coma (Jorgensen et al. 1996), i.e., in a diameter of about $8\farcs5$ at the distance of NGC 4993. Rather than using aperture corrections from a measurement of the central velocity dispersion, we measure the luminosity-weighted velocity dispersion directly from our MUSE data to be $\sigma = 171 \pm 2$ km s^{-1} (see also Figure 3 of Levan et al. 2017). This method allows us to tie our FP directly to that of Jorgensen et al. (1996), thus eliminating systematic uncertainties related to the approach adopted in determining the velocity dispersion.

4.2. FP Distance

The parameters used to determine the FP distance are summarized in Table 1. Calibrating the zero point of the FP to the Leo I group we can infer the distance to NGC 4993 as

$$D = 10^{-\log R_e + 1.24 \log \sigma - 0.82 \langle I_r \rangle_e + 2.194}(1 + z_{\mathrm{cosmic}})^2 \ \mathrm{Mpc} \quad (5)$$

(Hjorth & Tanvir 1997), where the last term corrects the angular diameter distance to luminosity distance. The resulting distance is 44.0 Mpc.

4.3. Uncertainties

The measurement of the effective radius is subject to systematic uncertainties due to the nuclear spiral arms, residuals at larger radius, and difficulty in determining the true background level. We estimate the uncertainty in R_e is about $1\farcs5$. The combination of R_e and $\langle I_r \rangle_e$ in Equation (1) is highly degenerate (Jorgensen et al. 1996) and so the FP distance is not very sensitive to the uncertainty in R_e. The measurement of σ required no aperture correction since we integrate over R_e in the IFU data directly. We estimate that the uncertainty in σ is about 2 km s^{-1}. The uncertainties in R_e and σ lead to $\sim$2.1% and $\sim$1.4% uncertainties in the distance, in total 2.5% in the distance. Therefore, the observational uncertainties are negligible compared to the intrinsic scatter in the FP that amounts to 17% (Jorgensen et al. 1996), which we adopt as the uncertainty in the FP distance to NGC 4993, i.e., $D_{\mathrm{FP}} = 44.0 \pm 7.5$ Mpc.

5. Discussion

The two distance estimates obtained in this Letter are independent. One is based on a redshift and an assumed Hubble constant, and the other is based on a direct measurement of the distance. We can therefore combine the two distances to yield $D_{\mathrm{NGC\ 4993}} = 41.0 \pm 3.1$ Mpc. This is consistent with the independent distance obtained from the gravitational-wave signal, $D_{\mathrm{GW}} = 43.8^{+2.9}_{-6.9}$ Mpc (Abbott et al. 2017c).

As a sanity check, we can compare these estimates to a slightly different approach. Figure 5 presents an analysis of the Cosmicflows-2 catalog (Tully et al. 2013). We took all distances in a range ± 1000 km s^{-1} around v_{CMB} of NGC 4993 and 10° around its position. From a fitted linear model with intrinsic scatter, the estimated distance for NGC 4993 is $D_{\mathrm{CF-2}} = 36.2 \pm 2.8$ Mpc (the error includes intrinsic scatter). We tried narrower cuts in v_{CMB} and the position, and the estimate is stable to such variations. This approach is not entirely independent from the other electromagnetic distances derived here, so we do not include it in our final value.

In Section 3, we used the Riess et al. (2016) value of the Hubble constant, $H_0 = 73.24 \pm 1.74$ km s^{-1} Mpc^{-1}. Planck Collaboration et al. (2016) instead find $H_0 = 67.8 \pm 0.9$ km s^{-1} Mpc^{-1} in a ΛCDM cosmology. Using the Planck value for H_0 would increase our best estimate of the luminosity distance from 40.4 Mpc to 43.7 Mpc, a shift by $\sim$1 standard deviation. This sensitivity to H_0 again points to the utility of these high-accuracy redshift measurements coupled with

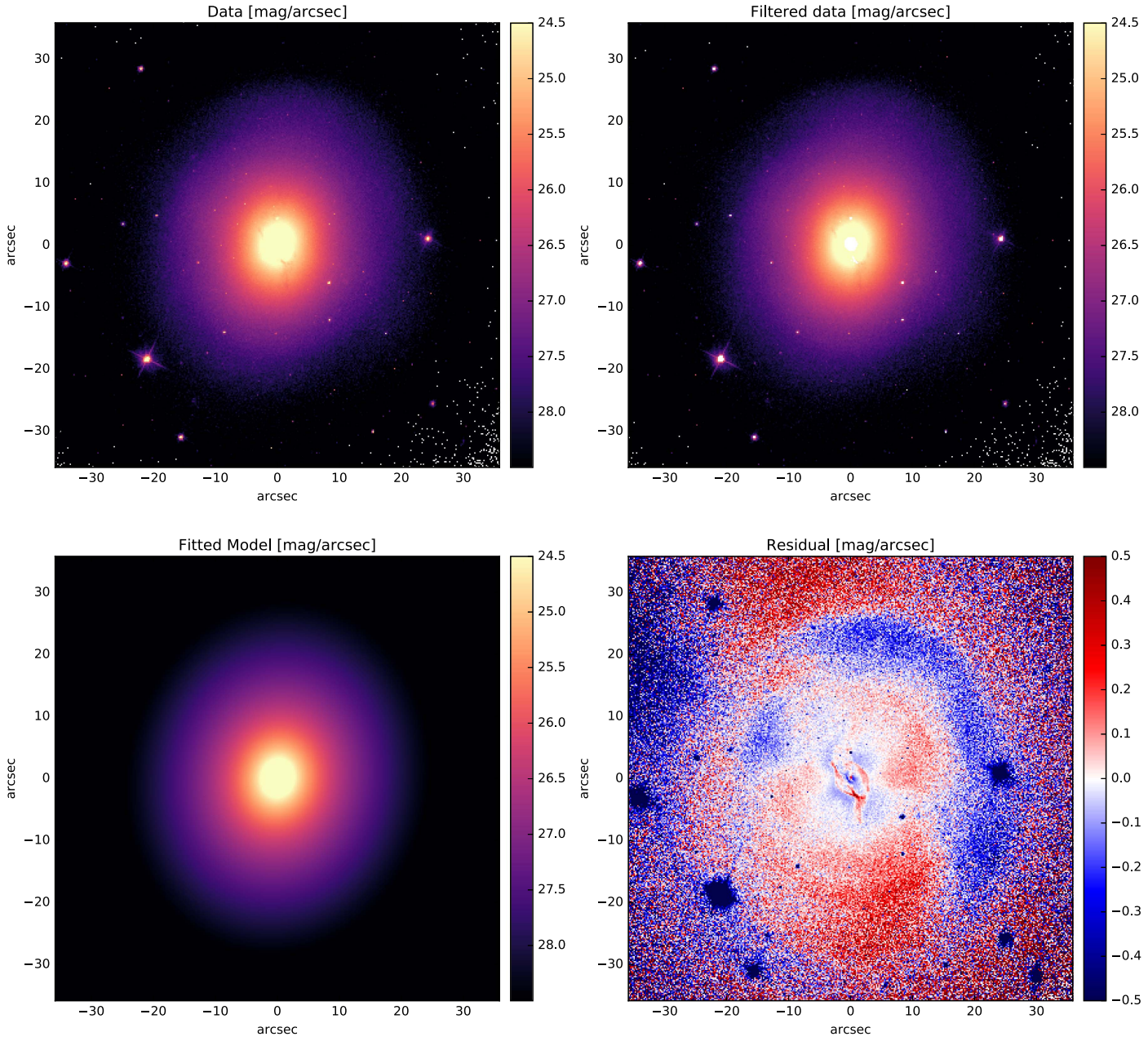

Figure 4. Fits to the F606W *HST* image of the host galaxy of GW170817. The top left panel shows the data, the top right panel shows the masked data, the bottom left panel shows the fitted model, and the bottom right panel shows the residuals between the data and the fit. North is up, and east is to the left.

Table 1
Redshift and Fundamental Plane Parameters of NGC 4993

$z_{\rm cosmic}$	R_e (arcsec)	$\log \langle I_r \rangle_e$ ($L_\odot$/pc^2)	σ (km s^{-1})
0.0098	15.5 ± 1.5	2.61 ± 0.06	171 ± 2

independent gravitational-wave distance measurements in the determination of H_0.

Other powerful distance indicators to distant early-type galaxies include surface brightness fluctuations (SBFs) and the globular cluster luminosity function (GCLF). Both methods are preferentially used at distances smaller than that of NGC 4993. For example, the GCLF peaks at $M_V \sim -7.5$ mag (Rejkuba 2012), i.e., at around F606W $\sim$ 25.5 at the distance of NGC 4993, about a magnitude shallower than the 2σ detection limit for point sources in the *HST* image (Levan et al. 2017). SBFs will be reported elsewhere.

6. Summary and Conclusions

We have obtained a new estimate of the distance to NGC 4993 based on two methods. (1) From a new measurement of its redshift with MUSE/VLT and an estimate of its peculiar velocity using CLUES constrained cosmological simulations we obtain $D_z = 40.4 \pm 3.4$ Mpc. (2) From new measurements of its velocity dispersion (with MUSE/VLT) and effective radius (*HST*; Table 1) we obtain an FP distance of $D_{\rm FP} = 44.0 \pm 7.5$ Mpc. Combined, these result in an "electromagnetic" distance of $D_{\rm NGC\ 4993} = 41.0 \pm 3.1$ Mpc. This compares well with the independent gravitational-wave

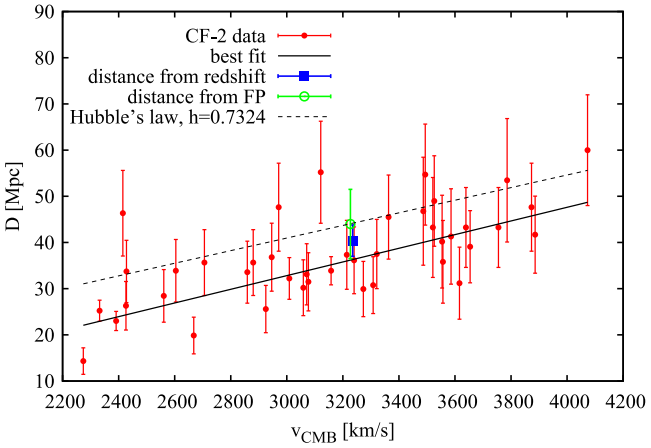

Figure 5. Distance vs. recession velocity in the CMB frame for Cosmicflows-2 galaxies. The best-fitting relation is consistent with the distance derived for NGC 4993 from the redshift and FP methods within the errors.

distance of $D_{GW} = 43.8^{+2.9}_{-6.9}$ Mpc. These results are summarized in Table 2.

The consistency between the electromagnetic and gravitational-wave distances lends credence to both avenues of determining distances and confirms that GW170817 occurred in NGC 4993.

There are at least two different ways in which the electromagnetically measured redshift to the host can lead to improved inference from gravitational-wave data. We can assume, as in Section 3.4, that the Hubble constant H_0 is known from other observations in order to provide better constraints on the distance. This distance estimate can then be fed in to gravitational-wave data analysis as a much tighter distance prior than the isotropic-in-volume prior $p(D) \propto D^2$ (Veitch et al. 2015). Better distance constraints can help break some of the strong correlations between parameters in the gravitational-wave signal, particularly the distance–inclination degeneracy (Cutler & Flanagan 1994; Aasi et al. 2013; Abbott et al. 2017c). Tighter constraints on the inclination angle of the binary's orbit relative to the line of sight can in turn aid in the interpretation of the electromagnetic transient. Alternatively, the electromagnetic redshift measurement and the gravitational-wave distance measurement can be combined to achieve an independent estimate of the Hubble constant, insensitive to the potential systematics of electromagnetic distance estimates (Schutz 1986; Abbott et al. 2017c).

The prospects for improving the electromagnetic distance to NGC 4993 are good. Future FP studies will benefit from studies of larger samples with MUSE/VLT, which will allow disentangling different velocity components in galaxies and perhaps a refined FP indicator. The uncertainties in the peculiar velocity will also diminish as we obtain a better understanding of cosmic flows, e.g., along the avenue presented in this work. Improved photometric parameters and extension to SBF and GCLF distance indicators are within reach with the *James Webb Space Telescope*.

R.W. thanks Vinicius Araújo Barbosa de Lima for his help in handling the simulation data. We thank the LIGO and Virgo Scientific Collaborations for sharing information prior to publication and for helpful comments on the manuscript. We thank the anonymous referee for a swift and insightful review. This work was supported by a VILLUM FONDEN Investigator grant to J.H. (project number 16599). A.J.L. is supported by STFC and the ERC (grant #725246). J.D.L. gratefully acknowledges support from STFC (ST/P000495/1). I.M. acknowledges partial support from STFC. C.G. acknowledges support from the Carlsberg Foundation. This work is based in part on observations collected at the European Organisation for Astronomical Research in the Southern Hemisphere under ESO programme 099.D-0668.

Facilities: Hubble Space Telescope, Very Large Telescope.
Software: ASTROPY (Astropy Collaboration 2013).

Table 2
Distance Estimates to NGC 4993

Method	Distance (Mpc)
Redshift	40.4 ± 3.4
Fundamental Plane	44.0 ± 7.5
Combined Electromagnetic (z+FP)	41.0 ± 3.1
Gravitational Waves	$43.8^{+2.9}_{-6.9}$

ORCID iDs

Jens Hjorth https://orcid.org/0000-0002-4571-2306

References

Aasi, J., Abadie, J., Abbott, B. P., et al. 2013, PhRvD, 88, 062001
Abbott, B. P., Abbott, R., Abbott, T. D., et al. 2017a, PhRvL, https://doi.org/10.1103/PhysRevLett.119.161101
Abbott, B. P., Abbott, R., Abbot, T. D., et al. 2017b, ApJL, https://doi.org/10.3847/2041-8213/aa91c9
Abbott, B. P., Abbott, R., Abbott, T. D., et al. 2017c, Natur, https://doi.org/10.1038/nature24471
Astropy Collaboration 2013, A&A, 558, A33
Coulter, D. A., Foley, R. J., Kilpatrick, C. D., et al. 2017, Sci, https://doi.org/10.1126/science.aap9811
Crook, A. C., Huchra, J. P., Martimbeau, N., et al. 2007, ApJ, 655, 790
Cutler, C., & Flanagan, É E. 1994, PhRvD, 49, 2658
Djorgovski, S., & Davis, M. 1987, ApJ, 313, 59
Fukugita, M., Shimasaku, K., & Ichikawa, T. 1995, PASP, 107, 945
Gottloeber, S., Hoffman, Y., & Yepes, G. 2010, arXiv:1005.2687
Hinshaw, G., Weiland, J. L., Hill, R. S., et al. 2009, ApJS, 180, 225
Hjorth, J., & Tanvir, N. R. 1997, ApJ, 482, 68
Jorgensen, I., Franx, M., & Kjaergaard, P. 1996, MNRAS, 280, 167
Kourkchi, E., & Tully, R. B. 2017, ApJ, 843, 16
Levan, A. J., Lyman, J. D., Tanvir, N. R., et al. 2017, ApJL, https://doi.org/10.3847/2041-8213/aa905f
Li, X., Hjorth, J., & Wojtak, R. 2014, ApJL, 796, L4
Makarov, D., & Karachentsev, I. 2011, MNRAS, 412, 2498
Pian, E., D'Avanzo, P., Benetti, S., et al. 2017, Natur, https://doi.org/10.1038/nature24298
Planck Collaboration, Ade, P. A. R., Aghanim, N., et al. 2016, A&A, 594, A13
Rejkuba, M. 2012, Ap&SS, 341, 195
Riess, A. G., Macri, L. M., Hoffmann, S. L., et al. 2016, ApJ, 826, 56
Schlafly, E. F., & Finkbeiner, D. P. 2011, ApJ, 737, 103
Schutz, B. F. 1986, Natur, 323, 310
Sirianni, M., Jee, M. J., Benítez, N., et al. 2005, PASP, 117, 1049
Sorce, J. G., Tully, R. B., Courtois, H. M., et al. 2014, MNRAS, 444, 527
Springob, C. M., Magoulas, C., Colless, M., et al. 2014, MNRAS, 445, 2677
Springob, C. M., Masters, K. L., Haynes, M. P., Giovanelli, R., & Marinoni, C. 2009, ApJS, 182, 474
Tanvir, N. R., Levan, A. J., González-Fernández, C., et al. 2017, ApJL, https://doi.org/10.3847/2041-8213/aa90b6
Tully, R. B., Courtois, H. M., Dolphin, A. E., et al. 2013, AJ, 146, 86
Tully, R. B., Courtois, H. M., & Sorce, J. G. 2016, AJ, 152, 50
Tully, R. B., Rizzi, L., Shaya, E. J., et al. 2009, AJ, 138, 323
Veitch, J., Raymond, V., Farr, B., et al. 2015, PhRvD, 91, 042003
Willick, J. A., Courteau, S., Faber, S. M., et al. 1997, ApJS, 109, 333